

COMPARISON AMONG UNSTRUCTURED HIGH RESOLUTION ALGORITHMS IN THE SOLUTION OF THE EULER EQUATIONS IN TWO-DIMENSIONS

Edisson Sávio de Góes Maciel^a

^aResearcher, Rua Demócrito Cavalcanti, 152, Afogados, Recife, Pernambuco, Brazil,
50750-080, edissonsavio@yahoo.com.br

Keywords: Yee, Warming and Harten algorithm, Harten algorithm, Yee and Kutler algorithm, Hughson and Beran algorithm, Euler equations and unstructured algorithms.

Abstract. The present work compares the Yee, Warming and Harten, the Harten, the Yee and Kutler and the Hughson and Beran schemes applied to the solution of aeronautical and aerospace problems. The schemes are of TVD (“Total Variation Diminishing”) flux difference splitting type and are second order accurate in space. The Euler equations in conservative form, employing a finite volume formulation and an unstructured spatial discretization, in two-dimensions, are solved. The time integration is performed by a Runge-Kutta method, second order accurate. The steady state physical problems of the supersonic flows along a ramp and around a blunt body configuration are studied. The results have demonstrated that the Harten scheme has presented more accurate results in the ramp problem, whereas the Hughson and Beran scheme has presented more accurate solutions in the blunt body problem. In the ramp problem, the Yee, Warming and Harten and the Yee and Kutler schemes predicted more severe pressure fields. The shock angle was best predicted by the Harten scheme, which presented a percentage error of 4.91%. In the blunt body problem, the pressure field generated by the Hughson and Beran scheme was the most severe. The stagnation pressure ahead of the configuration was best estimated by the Hughson and Beran scheme, which presented a percentage error of 3.7%. The best value of the lift coefficient was evaluated by the Yee, Warming and Harten and by the Yee and Kutler schemes. As can be observed, errors below 5.0% were obtained in the determination of the physical parameters of the two problems. The Harten scheme is the cheapest one, being approximately 27.5% cheaper than the Yee, Warming and Harten scheme, the most expensive. As final conclusion, it is not possible to highlight the best scheme in terms of these two example-cases, being necessary more studies. This is the purpose of the next paper to be written by this author.

1 INTRODUCTION

High resolution upwind schemes have been developed since 1959, aiming to improve the generated solution quality, yielding more accurate solutions and more robust codes. The high resolution upwind schemes can be of flux vector splitting type or flux difference splitting type. In the former case, more robust algorithms are yielded, while in the later case, more accuracy is obtained. Several studies were performed involving high resolution algorithms in the international literature, as for example:

Roe (1981) presented a work that emphasized that several numerical schemes to the solution of the hyperbolic conservation equations were based on exploring the information obtained in the solution of a sequence of Riemann problems. It was verified that in the existent schemes the major part of this information was degraded and that only certain solution aspects were solved. It was demonstrated that the information could be preserved by the construction of a matrix with a certain "U property". After the construction of this matrix, its eigenvalues could be considered as wave velocities of the Riemann problem and the U_L-U_R projections over the matrix's eigenvectors are the jumps which occur between intermediate stages.

Yee, Warming and Harten (1982) implemented a high resolution second order explicit method based on Harten's ideas. The method had the following properties: (a) the scheme was developed in conservation form to ensure that the limit was a weak solution; (b) the scheme satisfied a proper entropy inequality to ensure that the limit solution would have only physically relevant discontinuities; and (c) the scheme was designed such that the numerical dissipation produced highly accurate weak solutions. The method was applied to the solution of a quasi-one-dimensional nozzle problem and to the two-dimensional shock reflection problem, yielding good results. An implicit implementation was also investigated to one- and two-dimensional cases.

Harten (1983) developed a class of new finite difference schemes, explicit and with second order of spatial accuracy to calculation of weak solutions of the hyperbolic conservation laws. These schemes highly non-linear were obtained by the application of a first order non-oscillatory scheme to an appropriated modified flux function. The so derived second order schemes reached high resolution, while preserved the robustness property of the original non-oscillatory scheme.

Yee and Kutler (1985) presented a work which extended the Harten (1983) scheme to a generalized coordinate system, in two-dimensions. The method called "TVD scheme" by the authors was tested to the physical problem of a moving shock impinging a cylinder. The numerical results were compared with the MacCormack (1969) scheme, presenting good results.

Hughson and Beran (1991) proposed an explicit, second order accurate in space, TVD scheme to solve the Euler equations in axis-symmetrical form, applied to the studies of the supersonic flow around a sphere and the hypersonic flow around a blunt body. The scheme was based on the modified flux function approximation of Harten (1983) and its extension from the two-dimensional space to the axis-symmetrical treatment was developed. Results were compared to the MacCormack (1969) algorithm's solutions. High resolution aspects,

capability of shock capture and robustness properties of this TVD scheme were investigated.

On an unstructured algorithm context, Maciel (2007a) has presented a work involving the numerical comparison of the algorithms of Roe (1981) and of Harten (1983). The Euler equations in conservative form, employing a finite volume formulation and an unstructured spatial discretization, were solved. Both schemes were flux difference splitting ones and accurate solutions were expected. The time integration was performed by a Runge-Kutta method of five stages. Both schemes were upwind ones and first order accurate in space and second order accurate in time. The steady state physical problems of the transonic flow along a convergent-divergent nozzle and of the supersonic flows along a ramp and around a blunt body were studied. A spatially variable time step procedure was implemented to accelerate the convergence of the numerical schemes. The results have demonstrated that the Roe (1981) scheme has presented more severe pressure fields in the ramp and blunt body problems and a more accurate value of the stagnation pressure in the blunt body case than the Harten (1983) scheme. Still in this line of analysis, Maciel (2007b) has presented another work involving the numerical comparison of the Steger and Warming (1981) and of Van Leer (1982) algorithms. The Euler equations in conservative form, employing a finite volume formulation and an unstructured spatial discretization, were again solved. Both schemes were flux vector splitting ones and more robustness properties were expected. The time integration was again performed by a Runge-Kutta method of five stages. Both schemes were upwind ones and first order accurate in space and second order accurate in time. The same problems studied in Maciel (2007a) were analyzed in this work. The results have demonstrated that the Van Leer scheme presents more severe pressure fields in the ramp and in the blunt body problems, as well more accurate values in the determination of the shock angle, ramp problem, and of the stagnation pressure, blunt body problem, than the Steger and Warming scheme, recommending the former to project calculations.

In this work, the Yee, Warming and Harten (1982), the Harten (1983), the Yee and Kutler (1985) and the Hughson and Beran (1991) schemes are implemented, on a finite volume context and using an upwind and unstructured spatial discretization, to solve the Euler equations, in two-dimensions, and are compared with themselves. The implemented schemes are second order accurate in space. The time integration uses a Runge-Kutta method of five stages and is second order accurate in time. All schemes are applied to the solution of the steady state physical problems of the supersonic flows along a ramp and around a blunt body configuration. The algorithms are accelerated to the steady state solution using a spatially variable time step. The effective gains in terms of convergence ratio with this procedure are reported in Maciel (2005). The results have demonstrated that the Hughson and Beran (1991) scheme yields more accurate solutions than the other schemes.

An unstructured discretization of the calculation domain is usually recommended to complex configurations, due to the easily and efficiency that such domains can be discretized (Mavriplis, 1990, and Pirzadeh, 1991). However, the unstructured mesh generation question will not be studied in this work.

2 EULER EQUATIONS

The fluid movement is described by the Euler equations, which express the conservation of mass, of linear momentum and of energy to an inviscid medium, heat non-conductor and compressible, in the absence of external forces. In integral and conservative forms, these equations can be represented by:

$$\frac{\partial}{\partial t} \int_V Q dV + \int_S [(E_e)_x n_x + (F_e)_y n_y] dS = 0, \quad (1)$$

with Q written to a Cartesian system, V is the cell volume, n_x and n_y are the components of the normal vector to the flux face, S is the flux area, and E_e and F_e are the convective flux vector components. The Q , E_e and F_e vectors are represented by:

$$Q = \begin{Bmatrix} \rho \\ \rho u \\ \rho v \\ e \end{Bmatrix}, \quad E_e = \begin{Bmatrix} \rho u \\ \rho u^2 + p \\ \rho uv \\ (e + p)u \end{Bmatrix} \quad \text{and} \quad F_e = \begin{Bmatrix} \rho v \\ \rho uv \\ \rho v^2 + p \\ (e + p)v \end{Bmatrix}, \quad (2)$$

being ρ the fluid density; u and v the Cartesian components of the velocity vector in the x and y directions, respectively; e the total energy per fluid volume unity; and p the static pressure of the fluid medium.

In the studied problems, the Euler equations were nondimensionalized in relation to the freestream density, ρ_∞ , and in relation to the freestream speed of sound, a_∞ . Hence, the density is nondimensionalized in relation to ρ_∞ ; the u and v velocity components are nondimensionalized in relation to a_∞ ; and the pressure and the total energy are nondimensionalized in relation to the product $\rho_\infty (a_\infty)^2$. The matrix system of the Euler equations is closed with the state equation $p = (\gamma - 1)[e - 0.5\rho(u^2 + v^2)]$, assuming the ideal gas hypothesis. The total enthalpy is determined by $H = (e + p)/\rho$.

Equation (1) describes a relation in which the time rate of variation of the Q state vector, inside a V volume, is balanced by the net convective flux which crosses the S boundary surface. The calculation domain is divided in a great number of triangular cells and the Eq. (1) is applied to each cell.

3 YEE, WARMING AND HARTEN (1982) ALGORITHM

The Yee, Warming and Harten (1982) algorithm, second order accurate in space, is specified by the determination of the numerical flux vector at “ I ” interface.

Following a finite volume formalism, which is equivalent to a generalized coordinate system, the right and left cell volumes, as well the interface volume, necessary to a coordinate change, are defined by:

$$V_R = V_{ne}, \quad V_L = V_i \quad \text{and} \quad V_I = 0.5(V_R + V_L), \quad (3)$$

where “ R ” and “ L ” represent right and left states, respectively, and “ ne ” represent a neighbor

volume to the “*i*” volume. In this work, it was adopted that “*L*” is associated to properties of a given “*i*” volume and “*R*” is associated to properties of the “*ne*” neighbor volume. The cell volume on an unstructured context is defined by:

$$V_i = 0.5[(x_{n1}y_{n2} + y_{n1}x_{n3} + x_{n2}y_{n3}) - (x_{n3}y_{n2} + y_{n3}x_{n1} + x_{n2}y_{n1})], \quad (4)$$

with n_1 , n_2 and n_3 being the nodes of a given triangular cell. The description of the computational cell and its nodes, flux interfaces and neighbors are shown in Fig. 1.

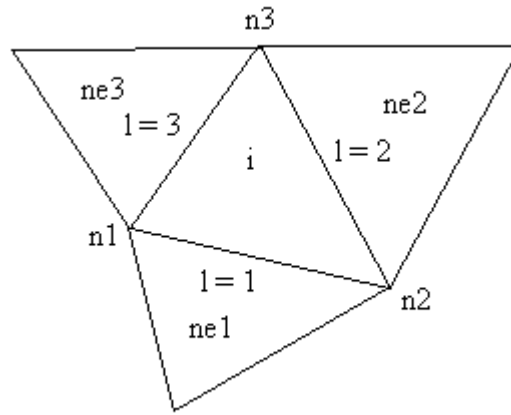


Figure 1. Schematic of a cell and its neighbors, nodes and flux interfaces.

The area components at the “*l*” interface are defined by:

$$S_x^l = n_x^l S^l \quad \text{and} \quad S_y^l = n_y^l S^l, \quad (5)$$

where n_x^l , n_y^l and S^l are defined as:

$$n_x^l = \Delta y_l / (\Delta x_l^2 + \Delta y_l^2)^{0.5}, \quad n_y^l = -\Delta x_l / (\Delta x_l^2 + \Delta y_l^2)^{0.5} \quad \text{and} \quad S^l = (\Delta x_l^2 + \Delta y_l^2)^{0.5}. \quad (6)$$

Expressions to Δx_l and Δy_l are given in Tab. 1.

Interface	Δx_l	Δy_l
$l = 1$	$x_{n2} - x_{n1}$	$y_{n2} - y_{n1}$
$l = 2$	$x_{n3} - x_{n2}$	$y_{n3} - y_{n2}$
$l = 3$	$x_{n1} - x_{n3}$	$y_{n1} - y_{n3}$

Table 1: Values of Δx_l and Δy_l .

The metric terms to this generalized coordinate system are defined as:

$$h_x = S_x^l / V_l, \quad h_y = S_y^l / V_l \quad \text{and} \quad h_n = S^l / V_l. \quad (7)$$

The properties calculated at the flux interface are obtained by arithmetical average or by Roe (1981) average. In the present work, the arithmetical average was used:

$$\rho_l = 0.5(\rho_R + \rho_L), u_l = 0.5(u_R + u_L), v_l = 0.5(v_R + v_L) \text{ and } H_l = 0.5(H_R + H_L); \quad (8)$$

$$a_l = \sqrt{(\gamma - 1)[H_l - 0.5(u_l^2 + v_l^2)]}, \quad (9)$$

where a_l is the speed of sound at the flux interface. The eigenvalues of the Euler equations, in the normal direction to the flux face, to the convective flux are given by:

$$q_{normal} = u_l h_x + v_l h_y, \lambda_1 = q_{normal} - a_l h_n, \lambda_2 = \lambda_3 = q_{normal} \text{ and } \lambda_4 = q_{normal} + a_l h_n. \quad (10)$$

The jumps of the conserved variables, necessary to the construction of the Yee, Warming and Harten (1982) dissipation function, are given by:

$$\Delta e = V_l(e_R - e_L), \Delta \rho = V_l(\rho_R - \rho_L), \Delta(\rho u) = V_l[(\rho u)_R - (\rho u)_L] \text{ and } \Delta(\rho v) = V_l[(\rho v)_R - (\rho v)_L]; \quad (11)$$

The α vectors to the “ l ” interface are calculated by the following expressions:

$$\alpha^1 = 0.5(aa - bb), \alpha^2 = \Delta \rho - aa, \alpha^3 = cc \text{ and } \alpha^4 = 0.5(aa + bb), \quad (12)$$

with:

$$aa = (\gamma - 1) / a_l^2 [\Delta e + 0.5(u_l^2 + v_l^2) \Delta \rho - u_l \Delta(\rho u) - v_l \Delta(\rho v)]; \quad (13)$$

$$bb = 1 / a_l [h'_x \Delta(\rho u) - (h'_x u_l + h'_y v_l) \Delta \rho + h'_y \Delta(\rho v)]; \quad (14)$$

$$cc = h'_x \Delta(\rho v) + (h'_y u_l - h'_x v_l) \Delta \rho - h'_y \Delta(\rho u); \quad (15)$$

$$h'_x = h_x / h_n \text{ and } h'_y = h_y / h_n. \quad (16)$$

The Yee, Warming and Harten (1982) dissipation function uses the right-eigenvector matrix of the normal to the flux face Jacobian matrix in generalized coordinates:

$$R_l = \begin{bmatrix} 1 & 1 & 0 & 1 \\ u_l - h'_x a_l & u_l & -h'_y & u_l + h'_x a_l \\ v_l - h'_y a_l & v_l & h'_x & v_l + h'_y a_l \\ H_l - h'_x u_l a_l - h'_y v_l a_l & 0.5(u_l^2 + v_l^2) & h'_x v_l - h'_y u_l & H_l + h'_x u_l a_l + h'_y v_l a_l \end{bmatrix}. \quad (17)$$

Two options to the ψ^m entropy function, responsible to guarantee that only relevant physical solutions are to be considered, are implemented aiming an entropy satisfying algorithm:

$$v_m = \Delta t \lambda_m = Z_m \text{ and } \psi_m = Z_m^2 + 0.25; \quad (18)$$

Or:

$$\psi_m = \begin{cases} |Z_m|, & \text{if } |Z_m| \geq \delta_f \\ 0.5(Z_m^2 + \delta_f^2) / \delta_f, & \text{if } |Z_m| < \delta_f \end{cases}, \quad (19)$$

where “ m ” varies from 1 to 4 (two-dimensional space) and δ_f assuming values between 0.1 and 0.5, being 0.2 the recommended value by Yee, Warming and Harten (1982). In the present studies, Eq. (18) was used to perform the numerical experiments.

The \tilde{g} function at the “ l ” interface is defined by:

$$\tilde{g}^m = 0.5(\psi_m - Z_m^2)\alpha^m. \quad (20)$$

The g numerical flux function, which is a limited function to avoid the formation of new extremes in the solution and is responsible to the second order accuracy of the scheme, is given by:

$$g_i^m = signal_m \times MAX(0.0; MIN(|\tilde{g}_i^m|, \tilde{g}_{i-1}^m \times signal_m)), \quad (21)$$

where $signal_m$ is equal to 1.0 if $\tilde{g}_i^m \geq 0.0$ and -1.0 otherwise.

The θ term, responsible to the artificial compressibility, as referred in the CFD community, which enhances the resolution of the scheme at discontinuities, is defined as follows:

$$\theta_i^m = \begin{cases} |\alpha_i^m - \alpha_{i-1}^m| / (|\alpha_i^m| + |\alpha_{i-1}^m|), & \text{if } |\alpha_i^m| + |\alpha_{i-1}^m| \neq 0.0 \\ 0.0, & \text{if } |\alpha_i^m| + |\alpha_{i-1}^m| = 0.0 \end{cases}, \quad (22)$$

The β vector at the “ l ” interface, which introduces the artificial compression term in the algorithm, is defined by the following expression:

$$\beta_m = 1.0 + \omega_m MAX(\theta_i^m, \theta_{i+1}^m), \quad (23)$$

where ω_m assumes the following values: $\omega_1 = 0.25$ (non-linear field), $\omega_2 = \omega_3 = 1.0$ (linear field) and $\omega_4 = 0.25$ (non-linear field).

The numerical characteristic speed, φ_m , at the “ l ” interface, which is responsible to transport the numerical information associated to the g numerical flux function, is defined by:

$$\varphi_m = \begin{cases} (g_{i+1}^m - g_i^m) / \alpha^m, & \text{if } \alpha^m \neq 0.0 \\ 0.0, & \text{if } \alpha^m = 0.0 \end{cases}. \quad (24)$$

The entropy function is redefined considering φ_m and β_m : $Z_m = v_m + \beta_m \varphi_m$, and ψ_m is recalculated according to Eq. (18) or to Eq. (19). Finally, the Yee, Warming and Harten (1982) dissipation function, to second order accuracy in space, is constructed by the following matrix-vector product:

$$\{D_{YWH}\}_l = [R]_l \left\{ \frac{(\beta(g_i + g_{i+1}) - \psi\alpha)}{\Delta t_i} \right\}_l. \quad (25)$$

The convective numerical flux vector to the “ l ” interface is described by:

$$F_l^{(m)} = (E_l^{(m)} h_x + F_l^{(m)} h_y) V_l + 0.5 D_{YWH}^{(m)}, \quad (26)$$

with:

$$E_l^{(m)} = 0.5(E_R^{(m)} + E_L^{(m)}) \quad \text{and} \quad F_l^{(m)} = 0.5(F_R^{(m)} + F_L^{(m)}). \quad (27)$$

The time integration is performed by an explicit method, second order accurate, Runge-Kutta type of five stages and can be represented of generalized form by:

$$\begin{aligned} Q_i^{(0)} &= Q_i^{(n)} \\ Q_i^{(k)} &= Q_i^{(0)} - \alpha_k \Delta t_i / V_i \times C(Q_i^{(k-1)}), \\ Q_i^{(n+1)} &= Q_i^{(k)} \end{aligned} \quad (28)$$

with $k = 1, \dots, 5$; $\alpha_1 = 1/4$, $\alpha_2 = 1/6$, $\alpha_3 = 3/8$, $\alpha_4 = 1/2$ and $\alpha_5 = 1$. The contribution of the convective numerical flux vectors is determined by the C_i vector:

$$C_i^{(m)} = F_1^{(m)} + F_2^{(m)} + F_3^{(m)}. \quad (29)$$

4 HARTEN (1983) ALGORITHM

The Harten (1983) algorithm, second order accurate in space, follows the Eqs. (3) to (17). The next step is the definition of the entropy condition, which is defined by Eq. (18), v_m , and Eq. (19).

The \tilde{g} function at the “ l ” interface is defined according to Eq. (20) and the g numerical flux function is given by Eq. (21). The numerical characteristic speed ϕ_m at the “ l ” interface is defined according to Eq. (24).

The entropy function is redefined considering ϕ_m : $Z_m = v_m + \phi_m$, and ψ_m is recalculated according to Eq. (19). Finally, the Harten (1983) dissipation function, to second order spatial accuracy, is constructed by the following matrix-vector product:

$$\{D_{Harten}\}_l = [R]_l \left\{ (g_i + g_{i+1} - \psi\alpha) / \Delta t_i \right\}_l. \quad (30)$$

Equations (26), (27) and (29) are used to conclude the numerical flux vector of the Harten (1983) scheme and the time integration is performed by the Runge-Kutta method defined by Eqs. (28).

5 YEE AND KUTLER (1985) ALGORITHM

The Yee and Kutler (1985) algorithm, second order accurate in space, follows Eqs. (3) to (17). The next step consists in determining the θ function. This function is defined in terms of

the differences of the gradients of the characteristic variables to take into account discontinuities effects and is responsible to artificial compression:

$$\theta_i^m = \begin{cases} \frac{|\alpha_i^m - \alpha_{i-1}^m|}{\alpha_i^m + \alpha_{i-1}^m}, & \text{if } (\alpha_i^m + \alpha_{i-1}^m) \neq 0.0 \\ 0.0, & \text{if } (\alpha_i^m + \alpha_{i-1}^m) = 0.0 \end{cases} \quad (31)$$

The κ function at the “ l ” interface is defined as follows:

$$\kappa_m = 1/\delta \left(1 + \omega_m \text{MAX}(\theta_i^m, \theta_{i+1}^m) \right), \quad (32)$$

The g numerical flux function is determined by:

$$g_i^m = \text{signal}_m \times \text{MAX} \left(0.0; \text{MIN} \left(|\alpha_i^m|, \alpha_{i-1}^m \times \text{signal}_m \right) \right), \quad (33)$$

where signal_m assumes value 1.0 if $\alpha_i^m \geq 0.0$ and -1.0 otherwise. The numerical characteristic speed φ_m at the “ l ” interface is calculated by the following expression:

$$\varphi_m = \begin{cases} \kappa_m (g_{i+1}^m - g_i^m) / \alpha^m, & \text{if } \alpha^m \neq 0.0 \\ 0.0, & \text{if } \alpha^m = 0.0 \end{cases} \quad (34)$$

The ψ_l entropy function at the “ l ” interface is defined by:

$$\psi_m = (v_m + \varphi_m)^2 + 0.25, \quad (35)$$

with v_l defined according to Eq. (18). Finally, the Yee and Kutler (1985) dissipation function, to second order spatial accuracy, is constructed by the following matrix-vector product:

$$\{D_{\text{Yee/Kutler}}\}_l = [R]_l \{(\kappa(g_i + g_{i+1}) - \psi\alpha) / \Delta t_i\}_l. \quad (36)$$

Equations (26), (27) and (29) are used to conclude the numerical flux vector of Yee and Kutler (1985) scheme and the time integration is performed by the Runge-Kutta method defined by Eqs. (28).

6 HUGHSON AND BERAN (1991) ALGORITHM

The Hughson and Beran (1991) algorithm, second order accurate in space, follows the Eqs. (3) to (17). The next step consists in determining the g numerical flux function. To non-linear fields ($m = 1$ and 4), it is possible to write:

$$g_i^m = \begin{cases} \frac{\alpha_i^m \alpha_{i-1}^m + |\alpha_i^m \alpha_{i-1}^m|}{\alpha_i^m + \alpha_{i-1}^m}, & \text{if } (\alpha_i^m + \alpha_{i-1}^m) \neq 0.0 \\ 0.0, & \text{if } (\alpha_i^m + \alpha_{i-1}^m) = 0.0 \end{cases} \quad (37)$$

To linear fields ($m = 2$ and 3), it is possible to write:

$$g_i^m = signal_m \times MAX(0.0; MIN(\alpha_{i-1}^m, \alpha_i^m \times signal_m)), \quad (38)$$

where $signal_m$ assumes the value 1.0 if $\alpha_{i-1}^m \geq 0.0$ and -1.0 otherwise. After that, the Eqs. (18) and (19) are employed and the σ_m term is defined at the “ l ” interface as:

$$\sigma_m = 0.5(\psi_m - Z_m^2). \quad (39)$$

The φ_m numerical characteristic speed at the “ l ” interface is defined by:

$$\varphi_m = \begin{cases} \sigma_m (g_{i+1}^m - g_i^m) / \alpha^m, & \text{if } \alpha^m \neq 0.0 \\ 0.0, & \text{if } \alpha^m = 0.0 \end{cases}. \quad (40)$$

The entropy function is redefined considering φ_m : $Z_m = v_m + \varphi_m$ and ψ_m is recalculated according to Eq. (19). Finally, the Hughson and Beran (1991) dissipation function, to second order accurate in space, is constructed by the following matrix-vector product:

$$\{D_{Hughson / Beran}\}_l = [R]_l \left\{ \frac{[\sigma(g_i + g_{i+1}) - \psi\alpha]}{\Delta t_i} \right\}. \quad (41)$$

After that, Eqs. (26), (27) and (29) are used to conclude the numerical flux vector of the Hughson and Beran (1991) scheme and Eq. (28) is employed to perform the time integration.

7 SPATIALLY VARIABLE TIME STEP

The basic idea of this procedure consists in keeping constant the CFL number in all calculation domain, allowing, hence, the use of appropriated time steps to each specific mesh region during the convergence process. Hence, according to the definition of the CFL number, it is possible to write:

$$\Delta t_i = CFL(\Delta s)_i / c_i, \quad (42)$$

where CFL is the “Courant-Friedrichs-Lewy” number to provide numerical stability to the scheme; $c_i = \left[(u^2 + v^2)^{0.5} + a \right]_i$ is the maximum characteristic velocity of information propagation in the calculation domain; and $(\Delta s)_i$ is a characteristic length of information transport. On a finite volume context, $(\Delta s)_i$ is chosen as the minor value found between the minor centroid distance, involving the “ i ” cell and a neighbor, and the minor cell side length.

8 INITIAL AND BOUNDARY CONDITIONS

8.1 Initial condition

To the physical problems studied in this work, freestream flow values are adopted for all

properties as initial condition, in the whole calculation domain (Jameson and Mavriplis, 1986, and Maciel, 2002). Therefore, the vector of conserved variables is defined as:

$$Q_i = \left\{ 1 \quad M_\infty \cos \alpha \quad M_\infty \sin \alpha \quad \frac{1}{\gamma(\gamma-1)} + 0.5M_\infty^2 \right\}^T, \quad (43)$$

being M_∞ the freestream flow Mach number and α the flow attack angle.

8.2 Boundary conditions

The boundary conditions are basically of three types: solid wall, entrance and exit. These conditions are implemented in special cells named ghost cells.

(a) Wall condition: This condition imposes the flow tangency at the solid wall. This condition is satisfied considering the wall tangent velocity component of the ghost volume as equals to the respective velocity component of its real neighbor cell. At the same way, the wall normal velocity component of the ghost cell is equaled in value, but with opposite signal, to the respective velocity component of the real neighbor cell.

The pressure gradient normal to the wall is assumed be equal to zero, following an inviscid formulation. The same hypothesis is applied to the temperature gradient normal to the wall. The ghost volume density and pressure are extrapolated from the respective values of the real neighbor volume (zero order extrapolation), with these two conditions. The total energy is obtained by the state equation of a perfect gas.

(b) Entrance condition:

(b.1) Subsonic flow: Three properties are specified and one is extrapolated, based on analysis of information propagation along characteristic directions in the calculation domain (Maciel, 2002). In other words, three characteristic directions of information propagation point inward the computational domain and should be specified, to the subsonic flow. Only the characteristic direction associated to the “ (q_n-a) ” velocity can not be specified and should be determined by interior information of the calculation domain. The pressure was the extrapolated variable from the real neighbor volume, to the studied problems. Density and velocity components had their values determined by the freestream flow properties. The total energy per unity fluid volume is determined by the state equation of a perfect gas.

(b.2) Supersonic flow: All variables are fixed with freestream flow values, at the entrance.

(c) Exit condition:

(c.1) Subsonic flow: Three characteristic directions of information propagation point outward the computational domain and should be extrapolated from interior information. The characteristic direction associated to the “ (q_n-a) ” velocity should be specified because it penetrates the calculation domain (Maciel, 2002). In this case, the ghost volume’s pressure is specified by its initial value. Density and velocity components are extrapolated and the total energy is obtained by the state equation of a perfect gas.

(c.2) Supersonic flow: All variables are extrapolated from the interior domain due to the fact that all four characteristic directions of information propagation of the Euler equations point outward the calculation domain and, with it, nothing can be fixed.

9 RESULTS

Tests were performed in a CELERON - 1.5 GHz and 1.0 Gbytes of RAM memory microcomputer. As the interest of this work is steady state problems, one needs to define a criterion which guarantees that such condition was reached. The criterion adopted in this work was to consider a reduction of 4 orders in the magnitude of the maximum residue in the domain, a typical criterion in the CFD community. The residue to each cell was defined as the numerical value obtained from the discretized conservation equations. As there are four conservation equations to each cell, the maximum value obtained from these equations is defined as the residue of this cell. Thus, this residue is compared with the residue of the other cells, calculated of the same way, to define the maximum residue in the domain. The value used for γ was 1.4. To all problems, the attack angle adopted a value 0.0° .

The meshes used in the simulations were structured generated and posteriorly were transformed in meshes of triangles through specific subroutines implemented in the calculation algorithms, where the connectivity, neighboring, node coordinate and ghost volume tables were generated to the simulations. On this context, only the advantages of unstructured mesh generation were not verified; however, the unstructured algorithms could be tested on a context of unstructured spatial discretization. Table 2 presents the mesh data.

	Ramp	Blunt Body
	61x100	103x100
Cells	11,800	20,196
Nodes	6,100	10,300

Table 2: Computational data of the unstructured meshes.

9.1 Ramp physical problem

The ramp configuration and the ramp mesh are described in Figs. 2 and 3. A freestream Mach number of 2.0, characterizing a supersonic flow, was adopted as initial condition.

Figures 4 to 7 exhibit the pressure contours generated by the Yee, Warming and Harten (1982), the Harten (1983), the Yee and Kutler (1985) and the Hughson and Beran (1991) schemes. The Yee, Warming and Harten (1982) and the Yee and Kutler (1985) schemes predict more severe pressure fields than the Harten (1983) and the Hughson and Beran (1991) schemes, characterizing the formers as more conservative schemes.

Figures 8 to 11 exhibit the Mach number contours generated by the Yee, Warming and Harten (1982), the Harten (1983), the Yee and Kutler (1985) and the Hughson and Beran (1991) schemes, respectively.

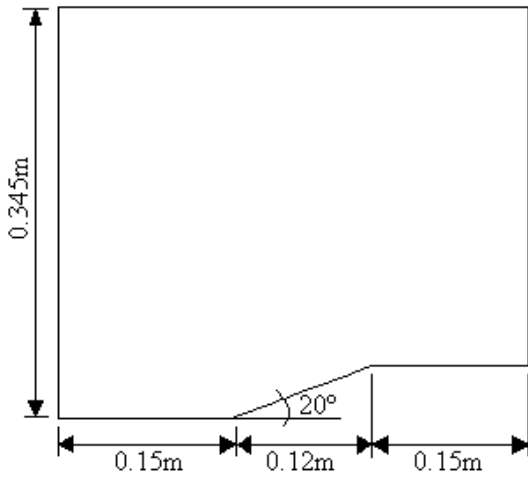


Figure 2. Ramp configuration.

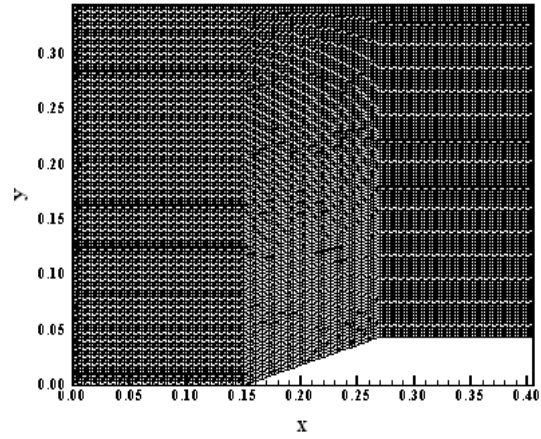


Figure 3. Ramp mesh.

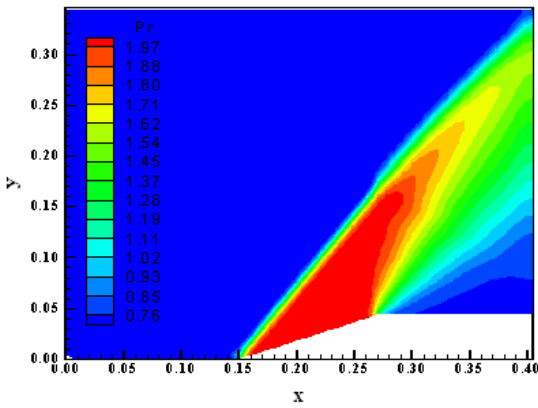


Figure 4. Pressure field (YWH).

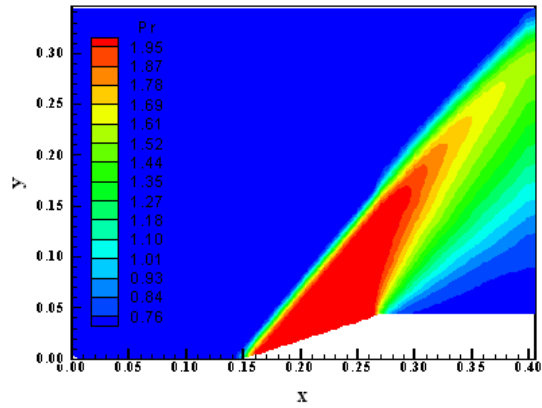


Figure 5. Pressure field (H).

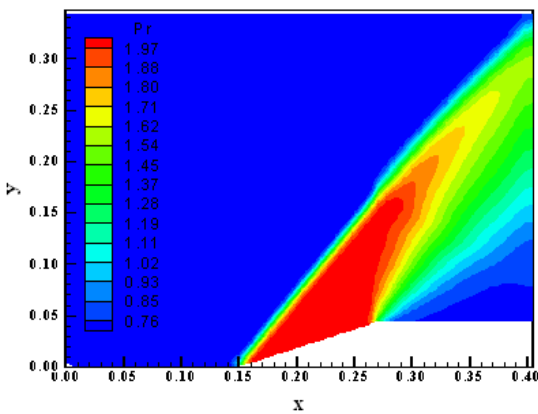


Figure 6. Pressure field (YK).

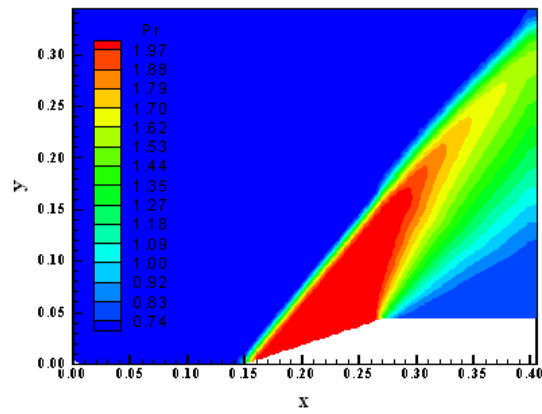


Figure 7. Pressure field (HB).

The Mach number field generated by the Hughson and Beran (1991) scheme is more intense

than those generated by the other schemes. The Hughson and Beran (1991) scheme presents some pre-shock oscillations, which elevate the values of the Mach number field above 2.0.

Figure 12 show the pressure distributions along the ramp obtained by the Yee, Warming and Harten (1982), the Harten (1983), the Yee and Kutler (1985) and by the Hughson and Beran (1991) schemes. They are compared with the oblique shock wave and the Prandtl-Meyer expansion wave theories. The shock and the expansion fan are appropriately formed and well solved by all schemes. The pressure plateau is over-predicted by all schemes. The Harten (1983) scheme presents the minimum over-prediction, capturing appropriately the shock plateau. The pressure at the end of the expansion fan is well detected by all schemes.

Figures 13 exhibit the convergence histories obtained with all schemes. The histories did not present oscillation, being all practically linear.

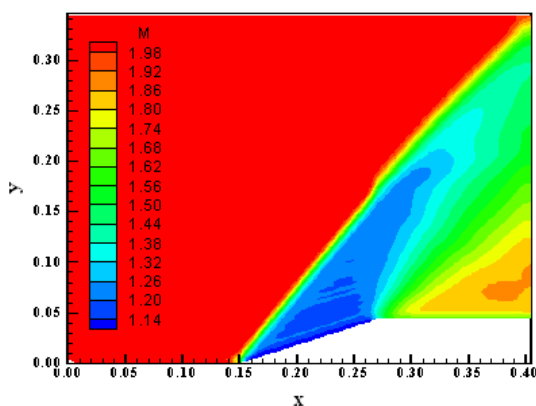


Figure 8. Pressure field (YWH).

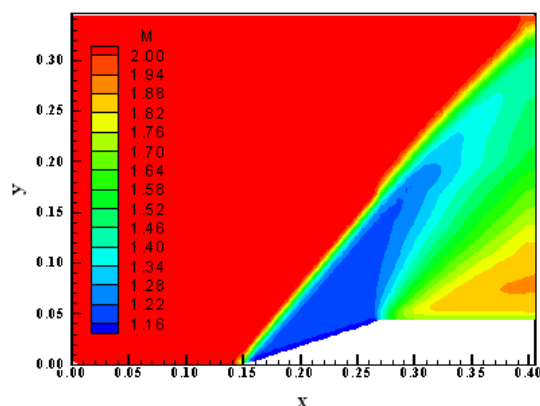


Figure 9. Pressure field (H).

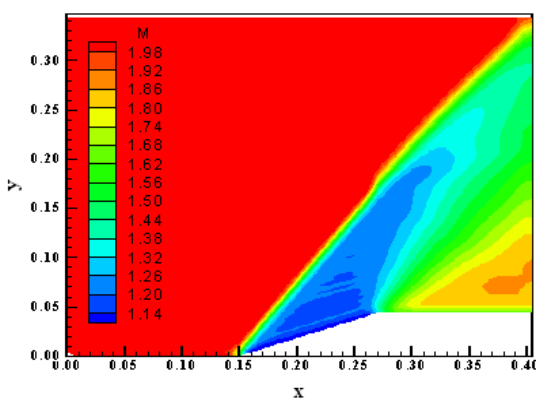


Figure 10. Mach number field (YK).

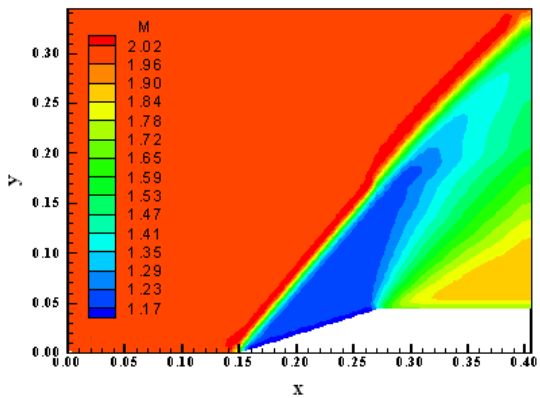


Figure 11. Mach number field (HB).

One way to quantitatively verify if the solutions to the ramp problem are satisfactory consists in determining the shock angle of the oblique shock wave, β , measured in relation to the initial direction of the flow field, obtained by each scheme.

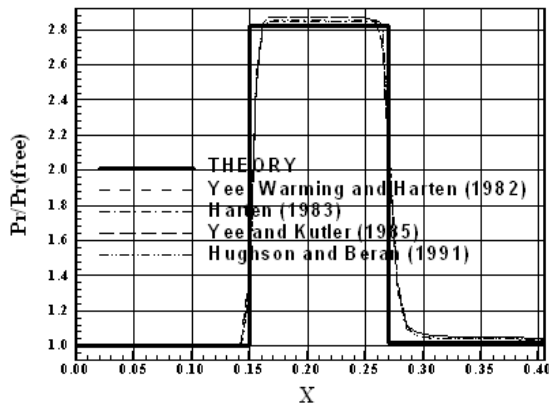


Figure 12. Pressure distributions.

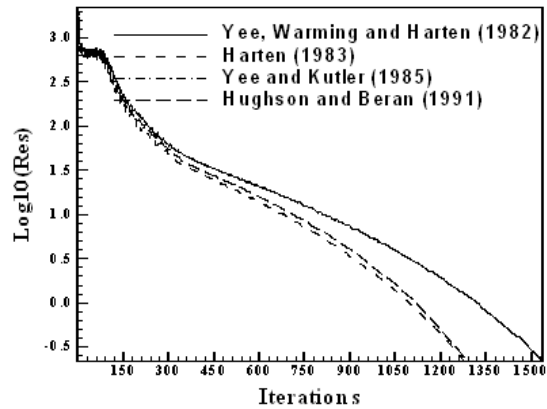


Figure 13. Convergence histories.

Anderson (1984) (pages 352 and 353) presents a diagram with values of the shock angle, β , to oblique shock waves. The value of this angle is determined as function of the freestream Mach number and of the deflection angle of the flow after the shock wave, ϕ . To $\phi = 20^\circ$ (ramp inclination angle) and to a freestream Mach number equals to 2.0, it is possible to obtain from this diagram a value to β equals to 53.0° . Using a transfer in Figures 4 to 7, it is possible to obtain in Tab. 3:

Algorithm:	β ($^\circ$):	Error (%):
Yee, Warming and Harten (1982)	50.0	5.66
Harten (1983)	50.4	4.91
Yee and Kutler (1985)	49.7	6.23
Hughson and Beran (1991)	50.1	5.47

Table 3: Shock angle and percentage error to the ramp problem.

The percentage errors indicate the Harten (1983) scheme as more accurate than the other schemes in the determination of the shock angle of the oblique shock wave.

9.2 Blunt body physical problem

Figures 14 and 15 exhibit the blunt body configuration and the respective mesh employed in the simulations, respectively. The entrance boundary is located at 20.0 times the nose ratio of the blunt body configuration in relation to the blunt body nose. The initial condition adopted for this problem used a freestream Mach number equals to 2.0 (supersonic flow).

Figures 16 to 19 show the pressure fields obtained by the Yee, Warming and Harten (1982), the Harten (1983), the Yee and Kutler (1985) and the Hughson and Beran (1991) schemes, respectively. The pressure field generated by the Hughson and Beran (1991) scheme is the most severe in relation to the other schemes.

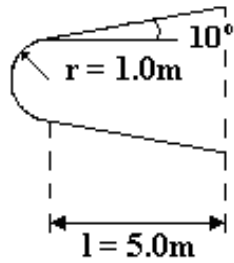


Figure 14. Blunt body configuration.

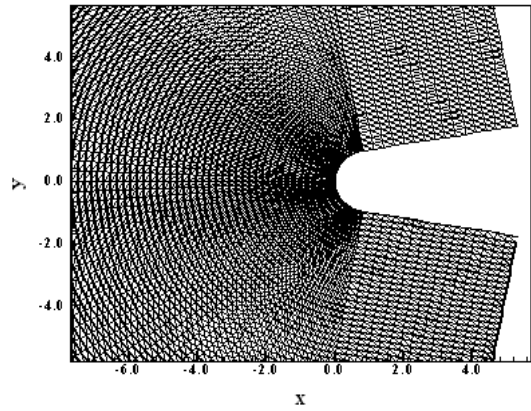


Figure 15. Blunt body mesh.

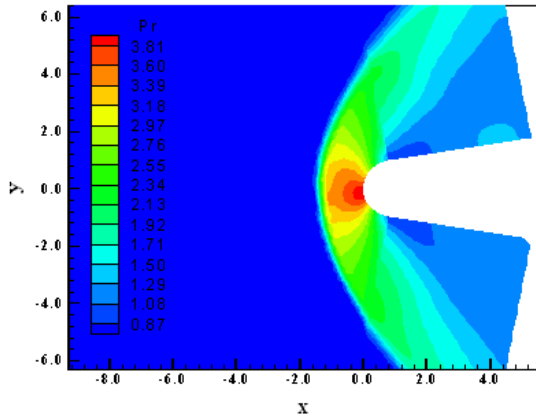


Figure 16. Pressure field (YWH).

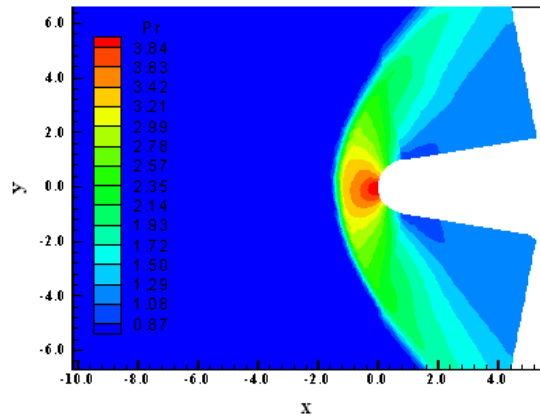


Figure 17. Pressure field (H).

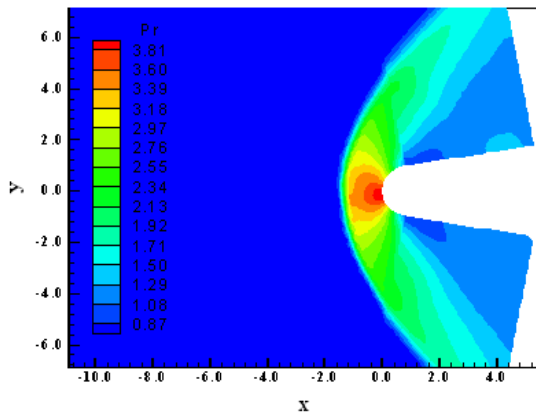


Figure 18. Pressure field (YK).

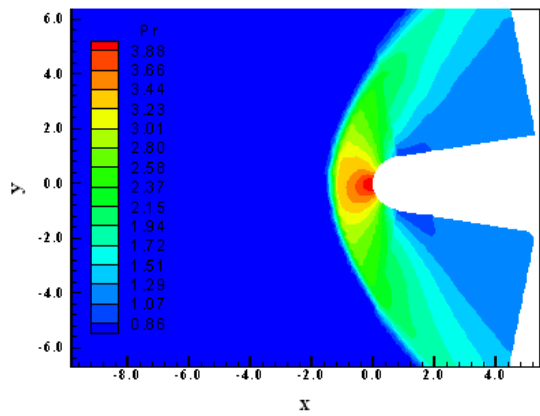


Figure 19. Pressure field (HB).

Figures 20 to 23 exhibit the Mach number contours obtained by the Yee, Warming Harten (1982), the Harten (1983), the Yee and Kutler (1985) and the Hughson and Beran (1991)

schemes, respectively. The Mach number field obtained with the Hughson and Beran (1991) scheme is the most intense. Figure 24 shows the $-C_p$ distributions obtained by all four schemes. No meaningful differences are perceptible in the solutions. Figure 25 exhibit the convergence histories obtained by all four schemes. The Yee, Warming and Harten (1982) and the Yee and Kutler (1985) schemes present are faster than the other schemes.

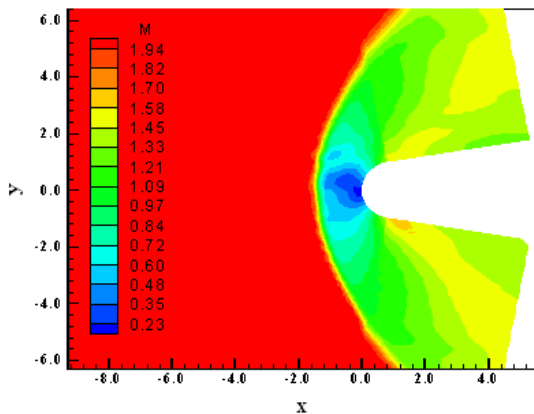


Figure 20. Mach number field (YWH).

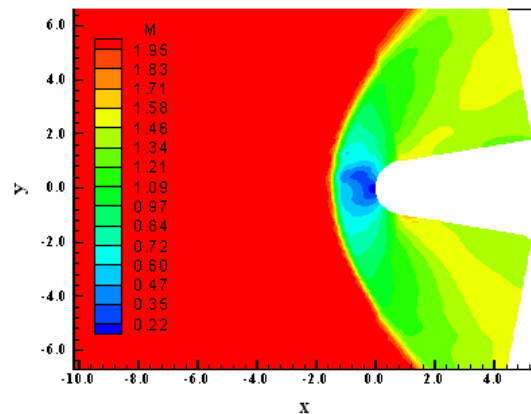


Figure 21. Mach number field (H).

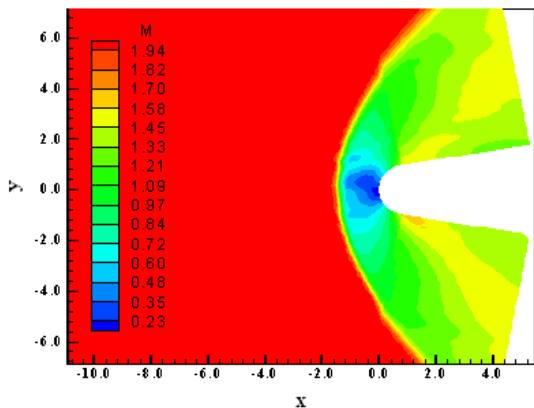


Figure 22. Mach number field (YK).

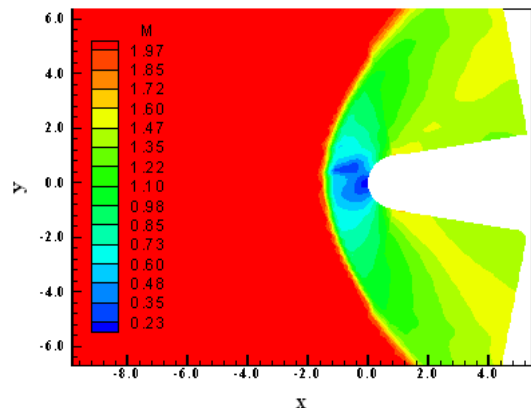


Figure 23. Mach number field (HB).

The lift and drag aerodynamic coefficients to this configuration, obtained by the schemes, are presented in Tab. 4. The lift and drag aerodynamic coefficients are defined as described in Anderson (1984). As the geometry is symmetrical and the attack angle of the simulations was considered equals to zero, the expected value to the aerodynamic coefficient of lift is equal to zero. The lift coefficient determined by the Yee, Warming and Harten (1982) and by the Yee and Kutler (1985) schemes are closer to the expected value.

Another possibility to quantitative analysis of both schemes is the determination of the stagnation pressure ahead of the configuration. Anderson (1984) presents a table of normal shock wave properties in its B Appendix. This table permits the determination of some shock wave properties as function of the freestream Mach number.

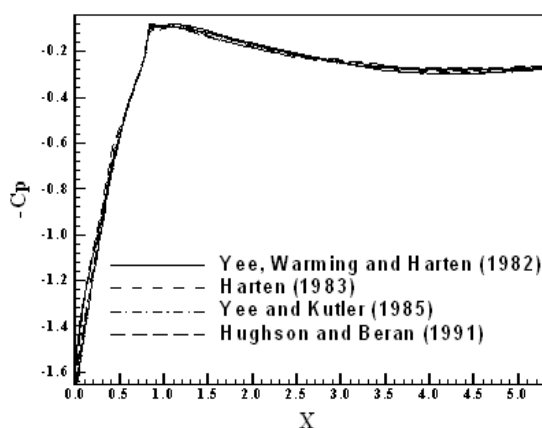
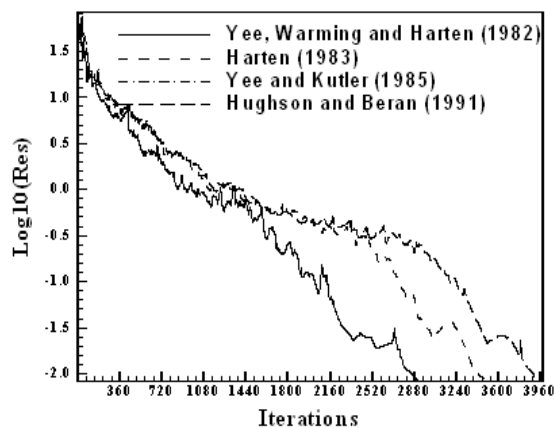
Figure 24. $-C_p$ distributions.

Figure 25. Convergence histories.

Algorithm:	c_L :	c_D :
Yee, Warming and Harten (1982)	1.668×10^{-3}	4.939×10^{-1}
Harten (1983)	2.497×10^{-3}	4.939×10^{-1}
Yee and Kutler (1985)	1.668×10^{-3}	4.939×10^{-1}
Hughson and Beran (1991)	5.686×10^{-3}	4.928×10^{-1}

Table 4: Aerodynamic coefficients of lift and drag to the blunt body problem.

In front of the blunt body configuration studied in this work, the shock wave presents a normal shock behavior, which permits the determination of the stagnation pressure, behind the shock wave, from the tables encountered in Anderson (1984). So it is possible to determine the ratio pr_0/pr_∞ from Anderson (1984), where pr_0 is the stagnation pressure in front of the configuration and pr_∞ is the freestream pressure (equals to $1/\gamma$ by the present nondimensionalization).

Hence, to this problem, $M_\infty = 2.0$ corresponds to $pr_0/pr_\infty = 5.64$ and remembering that $pr_\infty = 0.714$, it is possible to conclude that $pr_0 = 4.03$. Table 5 presents the values of the stagnation pressure obtained by each scheme and the respective percentage errors. Values of the percentage error indicate the Hughson and Beran (1991) scheme as the most accurate.

Algorithm:	pr_0 :	Error (%):
Yee, Warming and Harten (1982)	3.81	5.5
Harten (1983)	3.84	4.7
Yee and Kutler (1985)	3.81	5.5
Hughson and Beran (1991)	3.88	3.7

Table 5: Stagnation pressure and percentage error to the blunt body problem.

9.3 Numerical data

Table 6 presents the numerical data of the simulations. The most expensive algorithm is due to Yee, Warming and Harten (1982), whereas the cheapest is the Harten (1983) one. The Harten (1983) scheme is 27.5% cheaper than the Yee, Warming and Harten (1982) scheme. The percentage cheapness of the Harten (1983) algorithm, in relation to the Yee, Warming and Harten (1982) algorithm, is defined as $|Cost(YWH) - Cost(H)| \times 100 / Cost(H)$.

Algorithm:	Ramp		Blunt Body		Cost ⁽¹⁾ :
	CFL:	Iterations:	CFL:	Iterations:	
Yee, Warming and Harten (1982)	0.7	1,538	0.5	2,904	0.000102
Harten (1983)	0.8	1,285	0.4	3,473	0.000080
Yee and Kutler (1985)	0.7	1,538	0.5	2,904	0.000095
Hughson and Beran (1991)	0.8	1,294	0.4	3,925	0.000086

⁽¹⁾ Measured in seconds/per cell/per iteration.

Table 6: Numerical data of the simulations.

10 CONCLUSIONS

The present work aimed a comparison of the high resolution upwind schemes of Yee, Warming and Harten (1982), of Harten (1983), of Yee and Kutler (1985) and of Hughson and Beran (1991), applied to aerospace problems. All four schemes are second order accurate in space and are of TVD flux difference splitting type. The Euler equations, in conservative and integral forms, using a finite volume formulation and unstructured spatial discretization, were solved. All schemes were applied to the solution of the steady state physical problems of the supersonic flows along a ramp and around a blunt body configuration. A spatially variable time step was used to accelerate the convergence to the steady state condition. The effective gains in terms of convergence ratio with this procedure are reported in Maciel (2005).

The results have demonstrated that the Harten (1983) scheme has presented more accurate results in the ramp problem, whereas the Hughson and Beran (1991) scheme has presented more accurate solutions in the blunt body problem. In the ramp problem, the Yee, Warming and Harten (1982) and the Yee and Kutler (1985) schemes predicted more severe pressure fields. The shock angle was best predicted by the Harten (1983) scheme, which presented a percentage error of 4.91%. In the blunt body problem, the pressure field generated by the Hughson and Beran (1991) scheme was the most severe. The stagnation pressure ahead of the configuration was best estimated by the Hughson and Beran (1991) scheme, which presented a percentage error of 3.7%. The best value of the lift coefficient was evaluated by the Yee, Warming and Harten (1982) and by the Yee and Kutler (1985) schemes. The Harten (1983) scheme is the cheapest one, being approximately 27.5% cheaper than the Yee, Warming and Harten (1982) scheme, the most expensive.

As final conclusion, it is not possible to highlight the best scheme in terms of these two example-cases, being necessary more studies. This is the purpose of the next paper to be

written by this author involving these schemes.

REFERENCES

- Anderson, J. D., *Fundamentals of Aerodynamics*. McGraw-Hill, Inc., EUA, 563p, 1984.
- Harten, A., High Resolution Schemes for Hyperbolic Conservation Laws. *Journal of Computational Physics*, 49: 357-393, 1983.
- Hughson, M. C., and Beran, P. S., Analysis of Hyperbolic Blunt-Body Flows Using a Total Variation Diminishing (TVD) Scheme and the MacCormack Scheme. *AIAA 91-3206-CP*, 1991.
- Jameson, A., and Mavriplis, D., Finite Volume Solution of the Two-Dimensional Euler Equations on a Regular Triangular Mesh. *AIAA Journal*, 24: 611-618, 1986.
- MacCormack, R. W., The Effect of Viscosity in Hypervelocity Impact Cratering. *AIAA Paper 69-354*, 1969.
- Maciel, E. S. G., Simulação Numérica de Escoamentos Supersônicos e Hipersônicos Utilizando Técnicas de Dinâmica dos Fluidos Computacional. *Doctoral Thesis*, ITA, CTA, São José dos Campos, SP, Brazil, 258p, 2002.
- Maciel, E. S. G., Analysis of Convergence Acceleration Techniques Used in Unstructured Algorithms in the Solution of Aeronautical Problems – Part I. *Proceedings of the XVIII International Congress of Mechanical Engineering (XVIII COBEM)*, Ouro Preto, MG, Brazil, 2005.
- Maciel, E. S. G., Comparison Between the First Order Upwind Unstructured Algorithms of Roe and of Harten in the Solution of the Euler Equations in Two-Dimensions. *Proceedings of the XIX Congress of Mechanical Engineering (XIX COBEM)*, Brasília, DF, Brazil, 2007a.
- Maciel, E. S. G., Comparison Between the First Order Upwind Unstructured Algorithms of Steger and Warming and of Van Leer in the Solution of the Euler Equations in Two-Dimensions. *Proceedings of the XIX Congress of Mechanical Engineering (XIX COBEM)*, Brasília, DF, Brazil, 2007b.
- Mavriplis, D. J., Accurate Multigrid Solution of the Euler Equations on Unstructured and Adaptive Meshes. *AIAA Journal*, 28: 213-221, 1990.
- Pirzadeh, S., Structured Background Grids for Generation of Unstructured Grids by Advancing Front Method. *AIAA Paper 91-3233-CP*, 1991.
- Roe, P. L., Approximate Riemann Solvers, Parameter Vectors, and Difference Schemes. *Journal of Computational Physics*. 43: 357-372, 1981.
- Yee, H. C., and Kutler, P., Application of Second-Order-Accurate Total Variation Diminishing (TVD) Schemes to the Euler Equations in General Geometries. *NASA-TM-85845*, 1985.
- Yee, H. C., Warming, R. F., and Harten, A., A High-Resolution Numerical Technique for Inviscid Gas-Dynamic Problems with Weak Solutions. *Proceedings of the 8th International Conference on Numerical Methods in Fluid Dynamics*, E. Krause, Editor, Lecture Notes in Physics, Springer-Verlag, Berlin, Germany, 170: 546-552, 1982.